

Communication

# Ball Milling Effect on the CO<sub>2</sub> Uptake of Mafic and Ultramafic Rocks: A Review

Ioannis Rigopoulos <sup>1,2,\*</sup>, Ioannis Ioannou <sup>2</sup>, Andreas Delimitis <sup>3</sup>, Angelos M. Efstathiou <sup>4</sup> and Theodora Kyratsi <sup>1</sup>

<sup>1</sup> Department of Mechanical and Manufacturing Engineering, University of Cyprus, 1678 Nicosia, Cyprus; kyratsi@ucy.ac.cy

<sup>2</sup> Department of Civil and Environmental Engineering, University of Cyprus, 1678 Nicosia, Cyprus; ioannis@ucy.ac.cy

<sup>3</sup> Department of Mechanical and Structural Engineering and Materials Science, University of Stavanger, 4036 Stavanger, Norway; andreas.delimitis@uis.no

<sup>4</sup> Department of Chemistry, Heterogeneous Catalysis Lab, University of Cyprus, 1678 Nicosia, Cyprus; efstath@ucy.ac.cy

\* Correspondence: rigopoulos.ioannis@ucy.ac.cy; Tel.: +357-22-894512

Received: 14 September 2018; Accepted: 4 November 2018; Published: 7 November 2018



**Abstract:** Mineral carbonation is considered to be the most stable mechanism for the sequestration of CO<sub>2</sub>. This study comprises a comparative review of the effect of ball milling on the CO<sub>2</sub> uptake of ultramafic/mafic lithologies, which are the most promising rocks for the mineralization of CO<sub>2</sub>. Samples of dunite, pyroxenite, olivine basalt and of a dolerite quarry waste material were previously subjected to ball milling to produce ultrafine powders with enhanced CO<sub>2</sub> uptake. The optimum milling conditions were determined through selective CO<sub>2</sub> chemisorption followed by temperature-programmed desorption (TPD) experiments, revealing that the CO<sub>2</sub> uptake of the studied lithologies can be substantially enhanced via mechanical activation. Here, all these data are compared, demonstrating that the behavior of each rock under the effect of ball milling is predominantly controlled by the mineralogical composition of the starting rock materials. The ball-milled rock with the highest CO<sub>2</sub> uptake is the dunite, followed by the olivine basalt, the pyroxenite and the dolerite. The increased CO<sub>2</sub> uptake after ball milling is mainly attributed to the reduction of particle size to the nanoscale range, thus creating more adsorption sites per gram basis, as well as to the structural disordering of the constituent silicate minerals.

**Keywords:** ball milling; carbon capture and storage (CCS); CO<sub>2</sub> chemisorption; mineral carbonation; mafic rocks; quarry wastes; ultramafic rocks; ultrafine powders

## 1. Introduction

The alleviation of the environmental impacts caused by the increasing levels of human CO<sub>2</sub> emissions represents one of the greatest challenges of this century. This anthropogenic impact on the global carbon cycle is considered to be the main reason for the observed climate change over the past decades [1], which is probably irreversible on human timescales [2]. Therefore, the development of efficient technologies for carbon capture and storage (CCS) is crucial to alleviate the ongoing climate problem. This has stimulated research on the potential use of rocks that are abundant throughout the world for the removal of CO<sub>2</sub> from the atmosphere [3–6].

Mineral carbonation is a CCS technology that was initially proposed by Seifritz [7], which includes the conversion of CO<sub>2</sub> into carbonate minerals [8–10]. It requires the participation of divalent cations (Ca, Mg and Fe) that are mostly found in ultramafic and mafic rocks. These cations can react with CO<sub>2</sub>

to form carbonate minerals that are stable over geologic timescales (e.g., calcite, dolomite, magnesite, siderite—the formation of the latter is rare, but the presence of Fe can lead to the formation of ferro-magnesite (e.g., Santos et al. [11])). Mineral carbonation minimizes the risk of CO<sub>2</sub> leakage and facilitates its long-term and safe storage [12]. The conversion of CO<sub>2</sub> into carbonate minerals can be performed either in situ, by the injection of CO<sub>2</sub> into mafic and ultramafic rock formations [4,13], or ex situ, as part of an industrial process, after the mining and crushing/grinding of the rock material [3,9,14]. Although the major challenges of ex situ mineral carbonation are the scale of mining operations and the high energy consumption involved in the process [3], this method could potentially be an economically viable option for small to medium emitters ( $\leq 2.5$  Mt CO<sub>2</sub>) [15].

Mineral carbonation reactions are thermodynamically favored under natural conditions, but they are governed by their slow kinetics. Therefore, by accelerating these reactions, it will be possible to mitigate the atmospheric accumulation of CO<sub>2</sub> over reasonable timescales. Ex situ carbonation reactions can be accelerated by (i) grinding the rock materials, (ii) increasing the reaction temperature, (iii) increasing the CO<sub>2</sub> pressure, and (iv) dissolving the rock material in various solutions [16–19]. During the last decade, several studies have focused on the application of milling techniques to olivine [16,20–24]. However, only a few recent papers have focused on partially altered olivine-rich rocks [14,19,25,26], which are much more abundant on the Earth's surface compared to pure olivine. In addition, a number of studies have focused on the ex situ carbon mineralization of industrial wastes (e.g., mine tailings, construction waste), which could further contribute to the reduction of atmospheric CO<sub>2</sub> concentrations, thus economically benefiting many industries [10,27–31]. On the other hand, the mechanisms of mineral reactions in the presence of CO<sub>2</sub> remain not very well understood to a large extent, particularly for ultramafic and mafic mineral assemblages.

Considering that most studies have focused on the CO<sub>2</sub> sequestration properties of mechanically activated minerals rather than rocks, the aim of this paper is to compare the experimental results acquired by Rigopoulos et al. [19,25,32,33] on the effect of ball milling on the CO<sub>2</sub> uptake of a variety of ultramafic/mafic lithotypes, which can be found in large quantities around the world. The results are combined and discussed together in order to understand the optimum ball milling conditions of each lithology and their different reactivity towards CO<sub>2</sub>. The ultimate goal is to explain the different behavior of each rock type under the effect of mechanical activation and how this affects the CO<sub>2</sub> uptake of the final ultrafine powders.

## 2. Materials and Methods

### 2.1. Sample Selection and Preparation

A dunite, a pyroxenite, an olivine basalt and a dolerite have been studied in previous works [19,25,32,33]. All the samples originated from the Troodos ophiolite complex [34–36]. The dolerite was a waste material from an aggregate quarry.

The mineralogical and textural features of the dunite, pyroxenite and basalt were thoroughly studied by petrographic analysis of representative thin sections using a polarizing microscope. On the other hand, the mineralogical composition of the dolerite, which was collected in the form of quarry fines (grain size < 63  $\mu\text{m}$ ), was determined by powder X-ray diffraction analysis. Initially, the samples were ground with a stainless steel pulverizer (except for the dolerite, which was already fine-grained) and then sieved to obtain the 104–150  $\mu\text{m}$  size fraction. A portion of this size fraction was used as starting material, while the remainder was ball-milled to further reduce its grain size. The non-ball-milled size fraction is henceforth referred to as “unmilled”.

### 2.2. Mechanical Activation

Mechanical activation was performed using a Fritsch Pulverisette 6 planetary mono mill; this was used to produce nanoscale rock materials (see Tables 1 and 2). For scientific and engineering reasons, the term “nanoscale” signifies a size range of approximately 1 nm to 100 nm [37].

**Table 1.** Ball milling conditions and textural properties of the unmilled and ball-milled ultramafic rocks (data from Rigopoulos et al. [19,32]).

Rock Type/ Sample Code	Ball Milling Conditions		Textural Properties		
	Milling Time (h)	Type of Milling	BET ( $\text{m}^2 \text{g}^{-1}$ )	Specific Pore Volume ( $\text{cm}^3 \text{g}^{-1}$ )	Average Pore Diameter (nm)
Dunite					
SM15 *	-	-	6.8	0.011	5.4
BM30	1	Wet (10 wt% H <sub>2</sub> O)	24.5	0.048	6.5
BM31	2	Wet (10 wt% H <sub>2</sub> O)	36.9	0.055	4.9
BM41	4	Wet (10 wt% H <sub>2</sub> O)	45.9	0.059	4.2
BM42	8	Wet (10 wt% H <sub>2</sub> O)	52.2	0.052	3.9
BM26	1	Wet (10 wt% Ethanol)	29.5	0.097	11.2
BM27	2	Wet (10 wt% Ethanol)	38.0	0.104	9.3
BM34	4	Wet (10 wt% Ethanol)	47.7	0.109	7.9
BM35	8	Wet (10 wt% Ethanol)	32.5	0.089	9.0
BM44	1	Wet (50 wt% Ethanol)	25.2	0.081	11.4
BM36	2	Wet (50 wt% Ethanol)	30.3	0.104	12.2
BM38	4	Wet (50 wt% Ethanol)	35.7	0.121	11.8
BM39	8	Wet (50 wt% Ethanol)	41.5	0.170	13.7
BM45	12	Wet (50 wt% Ethanol)	51.9	0.173	11.4
BM40	16	Wet (50 wt% Ethanol)	49.9	0.157	10.9
BM46	20	Wet (50 wt% Ethanol)	64.6	0.179	9.3
Pyroxenite					
SMP1 *	-	-	1.8	0.005	9.7
BM3	1	Wet (10 wt% Ethanol)	12.8	0.034	9.7
BM8	1	Wet (50 wt% Ethanol)	11.8	0.017	5.3
BM9	2	Wet (50 wt% Ethanol)	17.7	0.047	9.0
BM10	4	Wet (50 wt% Ethanol)	23.3	0.067	9.5
BM13	2	Wet (10 wt% Ethanol)	15.1	0.030	6.7
BM14	4	Wet (10 wt% Ethanol)	27.2	0.044	6.7
BM16	8	Wet (50 wt% Ethanol)	32.7	0.088	8.7
BM18	8	Wet (10 wt% Ethanol)	48.9	0.071	4.8
BM20	16	Wet (50 wt% Ethanol)	42.3	0.123	9.9
BM24	20	Wet (50 wt% Ethanol)	59.9	0.209	11.2
BM25	12	Wet (10 wt% Ethanol)	59.0	0.092	5.1
BM32	24	Wet (50 wt% Ethanol)	67.7	0.180	8.4
BM33	32	Wet (50 wt% Ethanol)	53.7	0.175	10.5

\* Starting materials.

**Table 2.** Ball milling conditions and textural properties of the unmilled and ball-milled mafic rocks (data from Rigopoulos et al. [25,33]).

Rock Type/ Sample Code	Ball Milling Conditions		Textural Properties		
	Milling Time (h)	Type of Milling	BET ( $\text{m}^2 \text{g}^{-1}$ )	Specific Pore Volume ( $\text{cm}^3 \text{g}^{-1}$ )	Average Pore Diameter (nm)
Basalt					
SM1 *	-	-	9.0	0.014	6.4
BM1	1	Wet (10 wt% Ethanol)	40.2	0.081	7.3
BM2	1	Wet (10 wt% H <sub>2</sub> O)	34.1	0.041	4.1
BM5	1	Wet (50 wt% Ethanol)	31.2	0.076	8.9
BM6	2	Wet (50 wt% Ethanol)	42.9	0.078	6.4
BM7	4	Wet (50 wt% Ethanol)	58.9	0.106	6.2
BM11	2	Wet (10 wt% Ethanol)	64.3	0.085	4.6
BM12	4	Wet (10 wt% Ethanol)	55.0	0.081	6.2
BM15	8	Wet (50 wt% Ethanol)	44.3	0.104	8.7
Dolerite (quarry waste)					
SM16 *	-	-	8.4	0.015	7.0
BM47	1	Wet (50 wt% Ethanol)	16.3	0.028	7.2
BM48	2	Wet (50 wt% Ethanol)	20.2	0.046	8.3
BM49	4	Wet (50 wt% Ethanol)	27.0	0.115	14.9
BM50	8	Wet (50 wt% Ethanol)	28.8	0.145	18.1
BM51	12	Wet (50 wt% Ethanol)	28.1	0.121	14.1
BM52	16	Wet (50 wt% Ethanol)	29.6	0.115	13.7
BM53	20	Wet (50 wt% Ethanol)	32.9	0.151	16.0
BM54	26	Wet (50 wt% Ethanol)	32.4	0.094	10.9
BM56	32	Wet (50 wt% Ethanol)	34.8	0.111	11.3

\* Starting materials.

### 2.3. Characterization of Unmilled and Ball-Milled Samples

The unmilled and ball-milled rock materials were characterized by powder X-ray diffraction to investigate potential mineralogical transformations that might have occurred during ball milling, as well as by the BET method to determine their specific surface area ( $\text{m}^2 \text{g}^{-1}$ ), specific pore volume ( $\text{cm}^3 \text{g}^{-1}$ ) and average pore diameter (nm) (see Tables 1 and 2). In addition, the studied samples were characterized by scanning electron microscopy (SEM), conventional and high-resolution transmission electron microscopy (TEM and HRTEM), in combination with energy-dispersive X-ray spectroscopy (EDXS).

Furthermore, the temperature-programmed desorption (TPD) of  $\text{CO}_2$  in He carrier gas was performed in a specially designed gas flow system [38] in order to evaluate both the concentration ( $\mu\text{mol g}^{-1}$ ) of adsorbed  $\text{CO}_2$  on the basic (oxygen anionic) sites of the studied rock materials and the distribution of strength of  $\text{CO}_2$  adsorption due to the heterogeneity of the surface of the adsorbent material. The latter is related to the temperature of appearance of the  $\text{CO}_2$  desorption rate maximum in the TPD trace [39]. This technique was selected because it allows fast measurements of the  $\text{CO}_2$  uptake in a great variety of materials under different  $\text{CO}_2$  gas environments and temperatures. Furthermore, it provides the means to identify different adsorption states of  $\text{CO}_2$  and carbonate-types formed (surface/bulk) and quantify their respective amounts and binding strength with the solid. The applied  $\text{CO}_2$ -TPD technique allows the measurement of  $\text{CO}_2$  uptake with 5% experimental error [38].

## 3. Results and Discussion

### 3.1. Petrography

The dunite is a partially serpentinized lithology, the primary mineralogical composition of which includes mainly olivine ( $\text{Fo}_{90-93}$ ) (>90%) and disseminated Cr-spinel. Hydrothermal alteration resulted in the development of serpentine (<10%), as well as of minor amounts of talc and chlorite.

The pyroxenite is mainly composed of almost equal amounts of clinopyroxene (diopside) and orthopyroxene (enstatite). In addition, a small amount of forsterite-rich olivine is present; thus, this sample is classified as olivine websterite [40]. This lithology has been slightly affected by alteration processes, as indicated by the presence of minor amounts of chlorite and actinolite. Small amounts of opaque minerals are also present.

The olivine basalt is mainly composed of subhedral to euhedral olivine ( $\text{Fo}_{88-90}$ ) phenocrysts (~40%). The groundmass is principally characterized by the presence of elongated laths of clinopyroxene (augite) and the absence of plagioclase phenocrysts. Additionally, the groundmass contains abundant opaque minerals, while the interstitial glass has been devitrified mainly to chlorite (~20%). The development of chlorite, talc, serpentine, tremolite and actinolite indicate that this rock has been affected by ocean-floor metamorphic processes.

The primary mineralogy of the dolerite quarry waste material includes residual clinopyroxene (augite) and anorthite. The secondary minerals include significant amounts of chlorite (~25%), as well as actinolite, epidote, albite, quartz and calcite. Small amounts of magnetite crystals are also present.

### 3.2. Powder X-ray Diffraction (PXRD)

Powder X-ray diffraction (PXRD) analyses were acquired for the unmilled and ball-milled rocks, indicating that there is no mineralogical transformation due to the ball milling process. However, milling caused a substantial reduction in the intensity of all powder XRD peaks (compare Figure 1a,b). This became more evident with increasing milling time, as demonstrated by the negative correlation between the ball milling duration and the ratio of maximum intensity to mean background intensity ( $I_{\text{max}}/I_0$ ) (Figure 2). This suggests the structural disordering of the constituent silicate minerals, which is considered to be one of the most important factors for enhancing carbonation reactions [14,18,20,23,41].

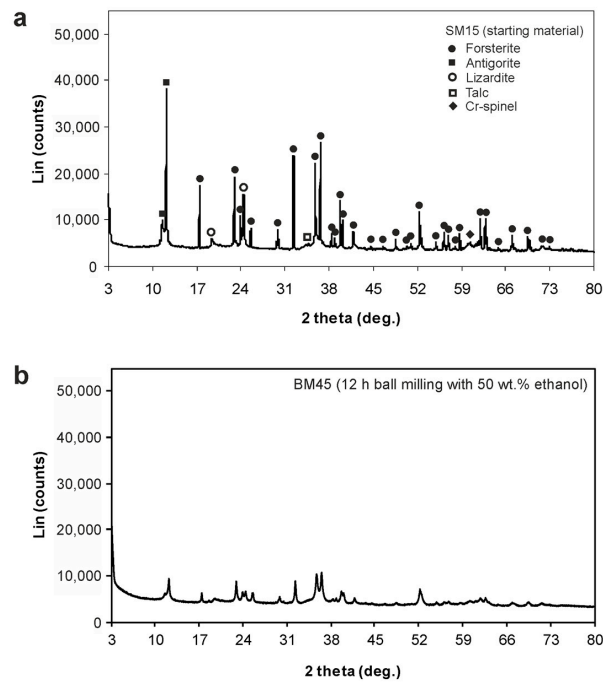


**Figure 1.** Powder X-ray diffraction patterns of (a) unmilled dunite, and (b) dunite after 12 h of ball milling with 50 wt% ethanol as PCA (modified from Rigopoulos et al. [19]).

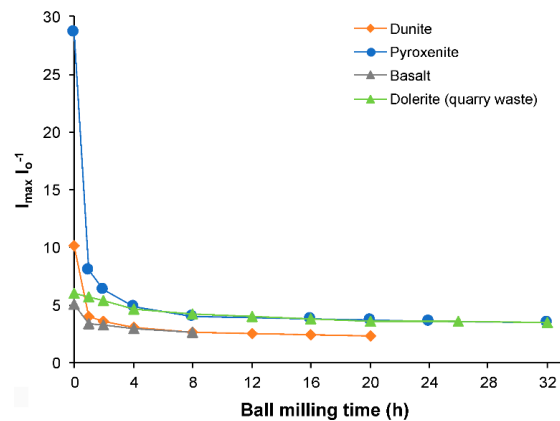


**Figure 2.** Relationships between the ball milling time (h) and the ratio of maximum intensity ( $I_{max}$ ) to mean background intensity ( $I_0$ ) acquired by the powder X-ray diffraction patterns of the unmilled and ball-milled rock samples (after milling with 50 wt% ethanol). The maximum intensity corresponds to the peak with the highest intensity in each XRD pattern, and the mean background intensity is the average of four background intensities (data from Rigopoulos et al. [19,25,32,33]).

In addition, PXRD studies revealed the different behavior of each lithology under the effect of mechanical deformation. The correlation between the ball milling duration and the  $I_{max}/I_0$  ratio revealed that the reduction in peak intensity during ball-milling is far more obvious in the pyroxenite, followed by the dunite, olivine basalt and dolerite (see Figure 2). It is suggested that the smallest reduction in peak intensity in the dolerite and basalt is attributed to the abundance of chlorite in these rock samples (see Section 3.1). Chlorite is a flexible mineral that tends to absorb the applied stress (e.g., see Rigopoulos et al. [42]), thereby increasing the resistance of the rock material to mechanical deformation. The dunite contains serpentine, the mechanical behavior of which is similar to that of chlorite [43]; however, its amount is notably smaller compared to that of chlorite in the basalt and dolerite (see Section 3.1). Regarding the pyroxenite, it shows the smallest degree of alteration (i.e., it contains only a minor amount of chlorite), which explains its high susceptibility to mechanical

deformation. All the aforementioned factors clearly support the idea that the exact mineralogical composition of each rock type comprises the main factor controlling the structural and morphological characteristics of the final ultrafine powders.

### 3.3. Surface Texture

The specific surface area (BET,  $\text{m}^2 \text{g}^{-1}$ ), the pore volume ( $\text{cm}^3 \text{g}^{-1}$ ) and the average pore diameter (nm) of the unmilled and ball-milled samples are summarized in Tables 1 and 2. Figure 3a–c shows the variation of these textural parameters, which clearly affects the  $\text{CO}_2$  uptake of rocks, with increasing milling duration, for the samples acquired after ball milling with 50 wt% ethanol as PCA. For all samples, the main increase of the BET specific surface area and pore volume occurred during the first 4 h of ball milling (Figure 3a,b), while longer milling times resulted in a smaller increase of these parameters or even in negative trends. The maximum value of the specific surface area for each rock type was acquired after different milling durations (Figure 3a); this is attributed to the distinct mineralogical and textural characteristics of each rock sample. Additionally, for the pyroxenite and basalt, an abrupt reduction of the BET specific surface area was observed after longer milling (Figure 3a); these negative trends are attributed to the agglomeration of nanoparticles that takes place after a few hours of ball milling [25,32]. Considering the abrupt reduction of specific surface area in the basalt after 8 h of ball-milling, longer milling was not performed in that case. Among the studied lithologies, only the dunite showed potential for a further increase of its specific surface area with additional milling (Figure 3a). However, this rock type was not subjected to milling beyond 20 h, since its high hardness could cause the contamination of the rock material from the vial and balls. Regarding the average pore diameter, a notable increase was recorded during the first few hours of milling; however, this parameter shows significant fluctuations over time (Figure 3c). This is likely attributed to the altered and multiphasic nature of the original rock samples, which are composed of primary and secondary minerals of different resistance to mechanical deformation.

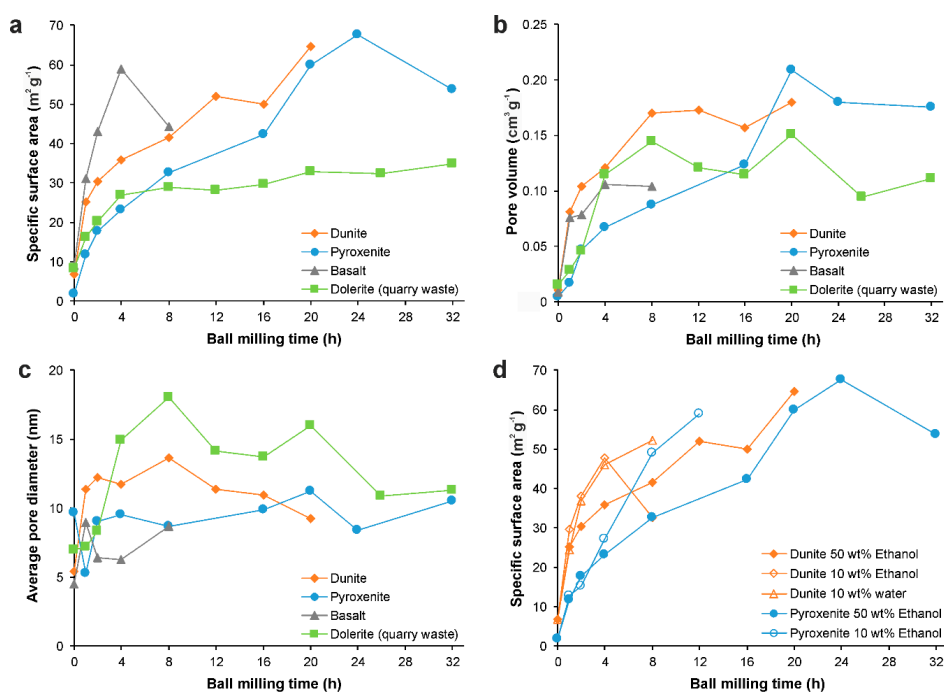


**Figure 3.** (a) BET ( $\text{m}^2 \text{g}^{-1}$ ) specific surface area, (b) pore volume ( $\text{cm}^3 \text{g}^{-1}$ ) and (c) average pore diameter (nm) plotted versus the ball milling time (h), for the milled rocks acquired after ball milling with 50 wt% ethanol. (d) BET ( $\text{m}^2 \text{g}^{-1}$ ) specific surface area plotted versus the ball milling time (h), for the dunite and pyroxenite samples acquired after milling with different types and quantities of PCA (data from Rigopoulos et al. [19,25,32,33]).

In the dunite and pyroxenite samples, additional ball milling was performed using 10 wt% ethanol and/or water as PCA (see Table 1). Although the reduction in the content of PCA from 50 wt% to 10 wt% led to a faster increase of the BET specific surface area with increasing milling time (Figure 3d), shorter milling times were performed at 10 wt% PCA (up to 8 h for the dunite and up to 12 h for the pyroxenite) in order to avoid contamination of the rock materials from the vial and balls, taking into account the high hardness of ophiolitic lithologies. The trends acquired (Figure 3d) indicate that a lower content of PCA tends to increase the intensity of the ball milling process, and consequently the reduction rate of particle size [14,19,25].

#### 3.4. Scanning Electron Microscopy (SEM)

SEM studies were performed on the mafic and ultramafic samples before and after the ball milling process. The unmilled rock materials are composed of large and angular particles (e.g., see Figure 4a), the size of which corresponds to the aperture size of the sieves (104–150  $\mu\text{m}$ ) that were used to acquire the fraction of the starting rock materials (see Section 2.1). The particles of the unmilled rock materials are covered by fine particles. The ball-milled materials are composed of particles that are substantially smaller, more rounded and uniform compared to the unmilled rocks (e.g., see Figure 4b). Detailed observations showed that the particle size of all samples decreases with increasing ball milling time (e.g., compare Figure 5a,b); this is in agreement with the notable increase of the specific surface area following mechanical activation (see Figure 3a). Furthermore, the milled samples usually contain agglomerated powder particles, the amount of which tends to increase with increasing ball milling duration (Figure 5c).

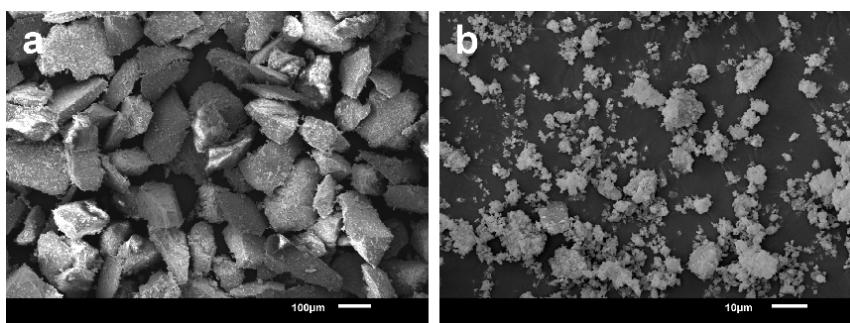


**Figure 4.** SEM images of the studied (a) unmilled (SM1), and (b) ball-milled olivine basalt for 8 h (BM15). The magnification in Figure 4a is significantly lower compared to that in Figure 4b.

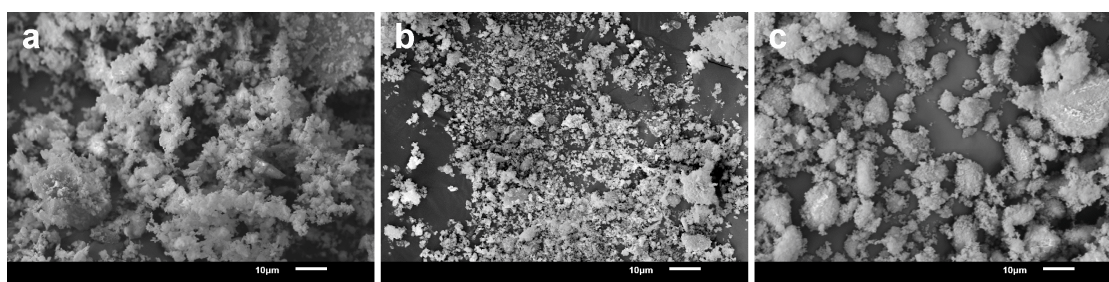


**Figure 5.** SEM images of the studied pyroxenite: (a) ball-milled for 1 h (BM8); (b) ball-milled for 4 h (BM10); (c) ball-milled for 32 h (BM33).

#### 3.5. Transmission Electron Microscopy (TEM and HRTEM)

TEM studies were performed on the ball-milled dunite and olivine basalt samples with the highest specific surface areas (samples BM46 and BM11, respectively; see Tables 1 and 2). These rocks are considered to be the most promising for mineral carbonation among the studied lithologies due to their high content in forsteritic olivine (see Section 3.1). Our observations confirmed the reduction of particle

size down to the nanoscale range after ball milling (Figure 6a,b). Specifically, the majority of the particle sizes in the milled dunite and olivine basalt with the highest specific surface areas range between 15–20 nm and 20–35 nm, respectively. EDXS point analyses were also obtained from numerous areas of these ultrafine samples, indicating that the forsterite content in olivine crystals ranges between 90% and 93% in the dunite, and between 88% and 90% in the basalt. Additionally, detailed observations confirmed that a number of particles are actually composed of smaller nanoparticles, confirming the agglomeration that takes place during ball milling; this is also in agreement with the observations acquired by SEM (see Figure 5c). Furthermore, in the basaltic sample, most of the olivine particles are still crystalline after ball milling (Figure 6c), indicating the high resistance of olivine to mechanical deformation. A greater variation of the olivine crystallinity was observed in the milled dunite. This sample, which was acquired after longer milling (i.e., 20 h for sample BM46) compared to the milled basalt (i.e., 2 h for sample BM11), contains a large quantity of highly disordered to amorphous olivine nanoparticles (Figure 6a); this is likely responsible for the higher CO<sub>2</sub> uptake of the milled dunite compared to the milled basalt (see Section 3.6). The higher degree of crystallinity of olivine in the basalt compared to the dunite is attributed to (i) the fact that the former has been subjected to a significantly shorter milling duration, and (ii) the presence of a significant amount of chlorite in the basaltic sample (see Section 3.1), which tends to absorb the applied stress during milling.

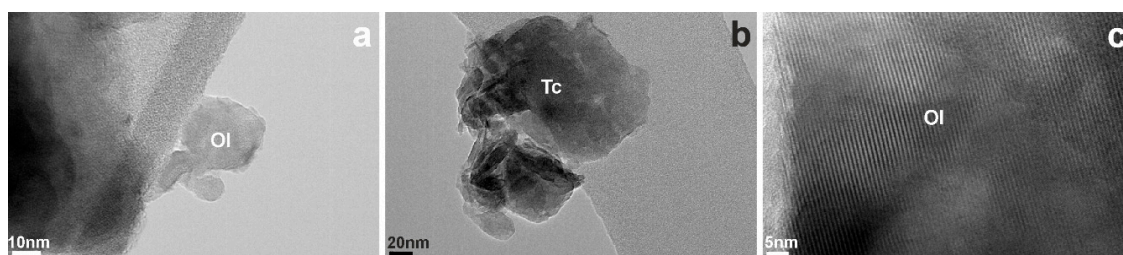


**Figure 6.** TEM images of the ball-milled dunite (BM46) and basalt (BM11) with the highest specific surface areas, showing: (a) the structural disordering of olivine in the dunite sample, as indicated by the amorphous-like contrast of the nanoparticles; (b) nanoparticles of talc in the basaltic sample; and (c) the existence of highly crystalline olivine in the basalt, as indicated by the lattice fringes (Ol: olivine, Tc: talc).

### 3.6. CO<sub>2</sub> Selective Chemisorption Followed by TPD

CO<sub>2</sub> temperature-programmed desorption (TPD) traces were acquired for the unmilled and ball-milled samples following the procedure described by Rigopoulos et al. [19,25,32,33]. For the dolerite samples, additional TPD traces were acquired without performing CO<sub>2</sub> chemisorption in order to estimate the desorbed amount of CO<sub>2</sub>, which is attributed to the calcite phase that pre-exists in the dolerite quarry waste (see Section 3.1).

The temperatures at which maximum desorption rates ( $T_{max}$ , °C) were observed and the total CO<sub>2</sub> uptake (or the equivalent desorbed amount) of the starting rock materials and ball-milled samples with the highest CO<sub>2</sub> uptake are summarized in Tables 3 and 4 (detailed results for all samples can be found in Rigopoulos et al. [19,25,32,33]). The estimated CO<sub>2</sub> uptake reflects the quantity of carbonate-type species (see Equation (1)) formed on the surface of each sample during chemisorption from a 5 vol% CO<sub>2</sub>/He gas mixture. Although the formation of these carbonate species usually takes place on the surface of each nanoparticle, this surface carbonation is the first critical step prior to bulk carbonation (i.e., diffusion of surface carbonates into the subsurface of the solid material).



The experimental results indicate that the unmilled dunite and basalt show a potential, albeit limited, CO<sub>2</sub> adsorption capacity (dunite: 40.1 μmol g<sup>-1</sup>, basalt: 56.3 μmol g<sup>-1</sup>; Table 3). On the other

hand, the estimated CO<sub>2</sub> uptake for the unmilled pyroxenite and dolerite are negligible (pyroxenite: 3.8 μmol g<sup>-1</sup>; Table 3, dolerite: 0.8 μmol g<sup>-1</sup>; Table 4). This difference is attributed to the abundance of forsteritic olivine in the dunite and basalt (see Section 3.1). The pyroxenite, on the other hand, is mainly composed of enstatite and diopside, which are less reactive towards CO<sub>2</sub> than olivine. Similarly, the negligible CO<sub>2</sub> uptake of the unmilled dolerite is assigned to its high content in hydrous minerals (mainly chlorite and actinolite), which are characterized by slow reaction rates [8].

It is worth noting that, although the unmilled basalt contains a notably smaller quantity of forsteritic olivine compared to the unmilled dunite (see Section 3.1), the former shows a higher CO<sub>2</sub> uptake (40.1 μmol g<sup>-1</sup> for the unmilled dunite and 56.3 μmol g<sup>-1</sup> for the unmilled basalt; Table 3). However, the ratio of the CO<sub>2</sub> uptake (μmol g<sup>-1</sup>) to the BET specific surface area (m<sup>2</sup> g<sup>-1</sup>) of these samples is similar (5.9 μmol m<sup>-2</sup> for the unmilled dunite and 6.3 μmol m<sup>-2</sup> for the unmilled basalt; Table 3), implying that their different values of CO<sub>2</sub> uptake are mainly attributed to their different values of specific surface area and not of CO<sub>2</sub> adsorption site density (number of sites per surface area). Considering that the grain size of both aforementioned samples is similar (i.e., 104–150 μm; see Section 2.1), it can be suggested that the higher BET value of the basalt is attributed to its multiphasic nature, which creates more complex grain boundaries compared to those of the dunite. These observations are also consistent with the experimental results reported by Sissman et al. [44].

**Table 3.** Peak maximum desorption temperatures ( $T_{\max}$ ) and amounts of CO<sub>2</sub> uptake (μmol g<sup>-1</sup>) (after chemisorption from a 5 vol% CO<sub>2</sub>/He gas mixture) estimated from CO<sub>2</sub>-TPD experiments for the starting dunite, basalt and pyroxenite, and the ball-milled samples with the highest CO<sub>2</sub> uptake. The CO<sub>2</sub> uptake per unit area of solid (μmol m<sup>-2</sup>) was also calculated after dividing the amount of CO<sub>2</sub> uptake per gram basis (μmol g<sup>-1</sup>) to the BET specific surface area (m<sup>2</sup> g<sup>-1</sup>) of each solid (BET values are given in Tables 1 and 2).

Sample Code	$T_{\max 1}$ (°C)	$T_{\max 2}$ (°C)	$T_{\max 3}$ (°C)	$T_{\max 4}$ (°C)	$T_{\max 5}$ (°C)	$T_{\max 6}$ (°C)	$T_{\max 7}$ (°C)	$T_{\max 8}$ (°C)	CO <sub>2</sub> Uptake (μmol g <sup>-1</sup> )	CO <sub>2</sub> Uptake (μmol m <sup>-2</sup> )	Reference
<i>Dunite</i>											
SM15 <sup>1</sup>	160	654	807	824	-	-	-	-	40.1	5.9	Rigopoulos et al. [19]
BM45 <sup>2</sup>	134	259	664	705	772	831	-	-	278.1	5.4	Rigopoulos et al. [19]
<i>Basalt</i>											
SM1 <sup>1</sup>	85	720	815	875	-	-	-	-	56.3	6.3	Rigopoulos et al. [25]
BM7 <sup>2</sup>	143	276	390	680	699	738	812	-	222.1	3.8	Rigopoulos et al. [25]
<i>Pyroxenite</i>											
SMP1 <sup>1</sup>	165	602	628	700	723	805	868	903	3.8	2.1	Rigopoulos et al. [32]
BM10 <sup>2</sup>	150	688	765	899	931	-	-	-	155.6	6.7	Rigopoulos et al. [32]

<sup>1</sup> Starting material, <sup>2</sup> ball-milled sample with the highest CO<sub>2</sub> uptake.

**Table 4.** Peak maximum desorption temperatures ( $T_{\max}$ ) and amounts of desorbed CO<sub>2</sub> (μmol g<sup>-1</sup>) (after chemisorption from a 5 vol% CO<sub>2</sub>/He gas mixture [Chem.], and without chemisorption [No chem.]) estimated from CO<sub>2</sub>-TPD experiments for the starting dolerite and the ball-milled dolerite with the highest CO<sub>2</sub> uptake. The CO<sub>2</sub> uptake (μmol g<sup>-1</sup>), which reflects the quantity of carbonate species formed on the surface of the samples following chemisorption, is the difference between the amounts of desorbed CO<sub>2</sub> after chemisorption and without chemisorption. The CO<sub>2</sub> uptake per unit area of solid (μmol m<sup>-2</sup>) was also calculated after dividing the amount of CO<sub>2</sub> uptake per gram basis (μmol g<sup>-1</sup>) to the BET specific surface area (m<sup>2</sup> g<sup>-1</sup>) of each solid (BET values are given in Table 2).

Sample Code		$T_{\max 1}$ (°C)	$T_{\max 2}$ (°C)	$T_{\max 3}$ (°C)	$T_{\max 4}$ (°C)	$T_{\max 5}$ (°C)	$T_{\max 6}$ (°C)	Desorbed CO <sub>2</sub> (μmol g <sup>-1</sup> )	CO <sub>2</sub> Uptake (μmol g <sup>-1</sup> )	CO <sub>2</sub> Uptake (μmol m <sup>-2</sup> )	Reference
SM16 <sup>1</sup>	Chem.	133	783	-	-	-	-	337.6	0.8	0.1	Rigopoulos et al. [33]
	No chem.	770	-	-	-	-	-	336.8			
BM53 <sup>2</sup>	Chem.	138	275	677	730	790	873	541.9	96.9	2.9	Rigopoulos et al. [33]
	No chem.	605	727	783	880	-	-	445.0			

<sup>1</sup> Starting material, <sup>2</sup> ball-milled sample with the highest CO<sub>2</sub> uptake.

The CO<sub>2</sub> uptake of all samples was substantially enhanced after ball milling (Tables 3 and 4). The correlation between the ball milling duration and the estimated CO<sub>2</sub> uptake of the studied rock materials confirms that ball milling substantially improves the ability of the studied ultramafic and

mafic lithotypes to adsorb CO<sub>2</sub> (Figure 7). For the dunite, it is obvious that the addition of 50 wt% ethanol during the ball milling process results in higher CO<sub>2</sub> uptakes compared to the addition of 10 wt% ethanol or water (Figure 7), despite the faster increase in specific surface area with the latter (Figure 3d). A similar behavior was also observed for the pyroxenite, implying that the use of 50 wt% ethanol during milling results in the development of ultrafine rock materials with the highest CO<sub>2</sub> uptake (Figure 7). These findings are consistent with Ounoughene et al. [45], who reported that an increase of the ethanol/solid ratio results in an increase of the carbonation conversion. Furthermore, these results imply that the specific surface area is not the only parameter that controls the CO<sub>2</sub> uptake. Thus, although the enhanced CO<sub>2</sub> uptake of the ball-milled rock materials is attributed to a large extent to the reduction of their particle size to the nanoscale range, the structural disordering of their constituent silicate minerals should also be considered an additional reason for their improved CO<sub>2</sub> adsorption properties (see also Section 3.2). This explains the values of CO<sub>2</sub> uptake per unit surface area of solid ( $\mu\text{mol m}^{-2}$ ) reported in Tables 3 and 4. From these results, it becomes evident that the increase of specific surface area during milling is generally not proportional to the formation of new basic sites that promote the adsorption of CO<sub>2</sub>. This is attributed to the fact that most of the rock materials under investigation here (i.e., basalt, pyroxenite and dolerite) are composed of a significant number of different mineral phases (see Section 3.1), the behavior of which under the effect of mechanical deformation varies. In addition, previous studies have shown that ball milling tends to create a significant number of crystal defects, many of which do not favor the formation of carbonates [25]. The number of crystal defects that promote carbonation mainly depends on the exact mineralogical composition of the starting rock materials. It is worth highlighting that the only rock material studied here showing a relatively proportional increase of CO<sub>2</sub> uptake with increasing specific surface area is the dunite; this is attributed to the fact that this rock is primarily composed of only one mineral phase (i.e., forsteritic olivine).

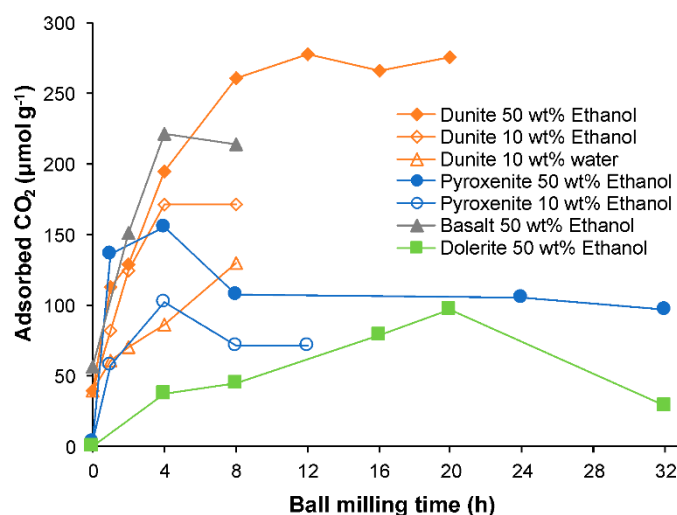


**Figure 7.** Adsorbed CO<sub>2</sub> ( $\mu\text{mol g}^{-1}$ ) versus ball milling time (h) for the unmilled and ball-milled dunite, pyroxenite, basalt and dolerite samples (data from Rigopoulos et al. [19,25,32,33]).

After ball milling, the dunite showed the highest enhancement of CO<sub>2</sub> uptake ( $278.1 \mu\text{mol g}^{-1}$  after 12 h of milling with 50 wt% ethanol), followed by the olivine basalt ( $222.1 \mu\text{mol g}^{-1}$  after 4 h of milling with 50 wt% ethanol), the pyroxenite ( $155.6 \mu\text{mol g}^{-1}$  after 4 h of milling with 50 wt% ethanol) and the dolerite waste material ( $96.9 \mu\text{mol g}^{-1}$  after 20 h of milling with 50 wt% ethanol) (Figure 7; Tables 3 and 4). However, it should be underlined that the milled basalt with the highest CO<sub>2</sub> uptake was acquired after a significantly shorter duration of ball milling (i.e., 4 h) compared to the milled dunite with the highest CO<sub>2</sub> uptake (i.e., 12 h). The latter indicates that the use of similar basaltic lithologies for the ex situ mineralization of CO<sub>2</sub> would result in a notably lower energy consumption.

Additionally, as can be seen in Figure 7, long hours of ball milling do not further improve the CO<sub>2</sub> adsorption properties of the studied mafic and ultramafic lithotypes. This is primarily attributed to the fact that the agglomeration of rock particles becomes more evident after many hours of ball milling (e.g., see Rigopoulos et al. [14]). It should also be highlighted that the CO<sub>2</sub> uptake of all samples decreases after a certain duration of ball milling (see Figure 7); this duration is not the same for all rock types, indicating that it mostly depends on their exact petrographic features.

The results of the CO<sub>2</sub>-TPD experiments further revealed that ball milling promotes the formation of strongly bound carbonate species, which generally tend to decompose at high temperatures (>600 °C). For example, Figure 8 shows that the main desorption peak of the milled dunite, the intensity of which is notably higher compared to the peak intensities of the unmilled rock material, appears at 772 °C (see also Table 3).

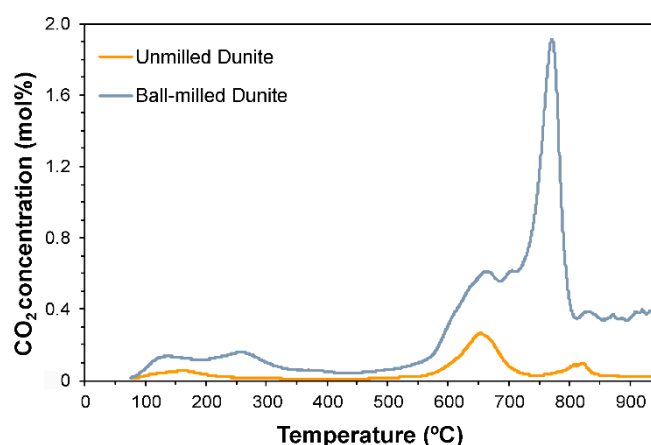


**Figure 8.** CO<sub>2</sub> temperature-programmed desorption (TPD) traces obtained under He flow for the unmilled dunite (SM15) and the ball-milled rock material with the highest CO<sub>2</sub> uptake (BM45). Adsorption conditions: 5 vol% CO<sub>2</sub>/He (50 N mL/min) at 500 °C for 30 min followed by cooling of the sample to 50 °C under the same gas mixture. Desorption conditions:  $Q_{He} = 50$  N mL/min,  $\beta = 30$  °C/min (data from Rigopoulos et al. [19]).

It should be underlined that the CO<sub>2</sub> uptake values of the studied rock materials, given in Tables 3 and 4, were acquired by performing gas–solid carbonation, where the reaction rates are very slow [8]. However, the CO<sub>2</sub> storage capacity could be substantially enhanced by performing aqueous carbonation [3]. Recent studies proved that ball milling can substantially enhance the weathering rate of ultramafic rocks in seawater, promoting the permanent storage of CO<sub>2</sub> as carbonate minerals [26]. These experiments resulted in a significant extent of mineral carbonation at ambient conditions.

#### 4. Practical Significance of the Results

The energy required to reduce the grain size of the initial rock materials to the nanoscale can notably reduce the carbon sequestration efficiency of the entire approach adopted in this study. According to O'Connor et al. [46], the energy required for the initial crushing step is estimated to be 2 kWh/ton. Grinding down to 75 μm adds another 11 kWh/ton, while further grinding down to 38 μm using ball mills adds ~70 kWh/ton [3]. Haug et al. [16], who performed milling in a laboratory planetary ball mill, reported that the first 10 min of milling are the most energy consuming, while the consumption of energy slightly decreases with increasing milling time. They also found that the planetary ball mill has large energy losses that are not related to the actual movement of the mill; thus, the energetic efficiency ranges between 30% and 54%. As such, the high energy consumption and cost associated with the production of ultrafine rock powders may hinder the large-scale application of this ex situ mineral carbonation approach. However, the incorporation of the ball milling process in the production of aggregates and other raw materials, rather than its execution as an isolated step

outside mines/quarries, could potentially reduce the operational energy consumption to practical levels [16]. Furthermore, the choice of certain lithologies with specific mineralogical composition (e.g., basalts) would lead to shorter durations of ball milling and subsequently to notably lower energy consumption, whilst the use of suitable quarry fines could further reduce the total energy required for the size reduction of the initial rock materials.

An advantage of the proposed carbon sequestration approach is that huge quantities of the studied ultramafic and mafic rock types can be found in many places throughout the world; this can substantially reduce the costs associated with the transportation of the feedstock. In addition, mafic and ultramafic rocks are considered as high-quality aggregate materials for the construction industry [47–49] and are quarried in many places around the globe. Therefore, the aggregate and construction industries could possibly use the fine waste material (original grain size < 63  $\mu\text{m}$ ) produced during mafic/ultramafic rock quarrying in order to sequester at least part of their own  $\text{CO}_2$  emissions. This could comprise a great financial advantage for these industries and would result in substantial environmental benefits. Subsequently, the end-products of mineral carbonation could be used by the construction industry as additives for the production of composite building materials (e.g., concretes, mortars), thereby increasing the efficiency of the overall approach.

An alternative option would be the use of ultrafine rock powders, before carbonation, as nano-additives in composite building materials, which rely on carbonation for hardening (e.g., mortars/renders). The enhancement of the carbonation reactions in the latter could result in the development of environmentally-friendly building materials with improved engineering properties; these will also have the potential to safely store  $\text{CO}_2$  in the form of carbonate minerals. It should also be underlined that the nano-sized mafic/ultramafic powders could be added in the building materials as a replacement to the cement or lime binder [50]; this would notably contribute to the reduction of human  $\text{CO}_2$  emissions, since huge quantities of  $\text{CO}_2$  are released into the atmosphere during the production of lime and cement [51,52]. Emphasis should be placed on the fact that the cement and lime industries could potentially integrate the development of ultrafine rock powders into their existing production lines, which already utilize ball mills; this would notably reduce the energy consumption related to the production of nanoscale rock materials.

## 5. Conclusions

The goal of this study was to compare and explain the different reactivity of a variety of ultrafine rock powders with  $\text{CO}_2$ , since there have been very limited similar studies to our knowledge. In summary, the comparative study of the effect of ball milling on the  $\text{CO}_2$  adsorption properties of a dunite, a pyroxenite, an olivine basalt and a dolerite quarry waste material revealed the following:

- Ball milling can be used for the development of ultrafine mafic/ultramafic powders with substantially enhanced  $\text{CO}_2$  uptake compared to the initial rock materials. This is due to the fact that the ball milling process modifies the crystal structure, surface morphology and size of the primary crystals of the minerals, thus increasing the number and strength of the surface basic sites that are responsible for the carbonation process;
- Prolonged ball milling resulted in a reduction of the  $\text{CO}_2$  uptake due to the increased agglomeration of nanoparticles;
- The use of 50 wt% ethanol as milling liquid resulted in the development of nanoscale powders with the highest  $\text{CO}_2$ -storage capacity;
- The optimum ball milling conditions, in terms of  $\text{CO}_2$  uptake, were not the same for all samples. The dunite showed the highest  $\text{CO}_2$  uptake after ball milling, followed by the olivine basalt, the pyroxenite and the dolerite;
- The exact petrographic characteristics (i.e., type of primary mafic minerals, degree of alteration, participation of flexible minerals) of each rock type are the main factors controlling the structural

and morphological characteristics, as well as the carbon sequestration efficiency, of the final ultrafine powders;

- The incorporation of the ball milling process in the production of aggregates and other raw materials, as well as the use of suitable quarry fines, could reduce to some extent the total energy required for the size reduction of the initial rock materials;
- The end-products of mineral carbonation could be used by the construction industry as additives. Alternatively, the ultrafine rock powders could be used, before carbonation, as nano-additives in composite building materials (in replacement to cement or lime), in order to enhance their carbonation process.

Future studies should focus on the reduction of the energy consumption related to the development of ultrafine powders, as well as on the carbon sequestration efficiency of this approach, by performing aqueous carbonation experiments under low temperature and pressure conditions.

**Author Contributions:** I.R., T.K. and I.I. designed the research. I.R. performed the experiments, analyzed the data and wrote the paper. A.M.E. provided access to the heterogeneous catalysis lab (CO<sub>2</sub> chemisorption/TPD) and contributed to the interpretation of the results. A.D. performed TEM studies along with EDXS analyses.

**Funding:** This work was carried out in the context of the Nanominerals Project, funded by the University of Cyprus, and the CO<sub>2</sub>NOR Project, which has received funding from the European Union's Horizon 2020 research and innovation programme under the Marie Skłodowska-Curie grant agreement No 654091. Additional financial support was provided by the Republic of Cyprus and the European Committee through the Cyprus Research Promotion Foundation (Project KOINA/M-ERA.NET/0316/04).

**Conflicts of Interest:** The authors declare no conflict of interest. The founding sponsors had no role in the design of the study; in the collection, analyses, or interpretation of data; in the writing of the manuscript, and in the decision to publish the results.

## References

1. Intergovernmental Panel on Climate Change (IPCC). *Climate Change 2014: Mitigation of Climate Change*; Cambridge University Press: Cambridge, UK; New York, NY, USA, 2014.
2. Solomon, S.; Plattner, G.K.; Knutti, R.; Friedlingstein, P. Irreversible climate change due to carbon dioxide emissions. *Proc. Nat. Acad. Sci. USA* **2009**, *106*, 1704–1709. [[CrossRef](#)] [[PubMed](#)]
3. Gerdemann, S.J.; O'Connor, W.K.; Dahlin, D.C.; Panner, L.R.; Rush, H. Ex situ aqueous mineral carbonation. *Environ. Sci. Technol.* **2007**, *41*, 2587–2593. [[CrossRef](#)] [[PubMed](#)]
4. Matter, J.M.; Stute, M.; Snæbjörnsdóttir, S.Ó.; Oelkers, E.H.; Gislason, S.R.; Aradóttir, E.S.; Sigfusson, B.; Gunnarsson, I.; Sigurdardóttir, H.; Gunnlaugsson, E.; et al. Rapid carbon mineralization for permanent disposal of anthropogenic carbon dioxide emissions. *Science* **2016**, *352*, 1312–1314. [[CrossRef](#)] [[PubMed](#)]
5. Power, I.M.; Harrison, A.L.; Dipple, G.M. Accelerating mineral carbonation using carbonic anhydrase. *Environ. Sci. Technol.* **2016**, *50*, 2610–2618. [[CrossRef](#)] [[PubMed](#)]
6. Snæbjörnsdóttir, S.Ó.; Gislason, S.R.; Galeczka, I.M.; Oelkers, E.H. Reaction path modelling of in-situ mineralisation of CO<sub>2</sub> at the CarbFix site at Hellisheidi, SW-Iceland. *Geochim. Cosmochim. Acta* **2018**, *220*, 348–366. [[CrossRef](#)]
7. Seifritz, W. CO<sub>2</sub> disposal by means of silicates. *Nature* **1990**, *345*, 486. [[CrossRef](#)]
8. Lackner, K.S.; Wendt, C.H.; Butt, D.P.; Joyce, E.L.; Sharp, D.H. Carbon dioxide disposal in carbonate minerals. *Energy* **1995**, *20*, 1153–1170. [[CrossRef](#)]
9. Oelkers, E.H.; Gislason, S.R.; Matter, J. Mineral carbonation of CO<sub>2</sub>. *Elements* **2008**, *4*, 333–337. [[CrossRef](#)]
10. Sanna, A.; Uibu, M.; Caramanna, G.; Kuusik, R.; Maroto-Valer, M. A review of mineral carbonation technologies to sequester CO<sub>2</sub>. *Chem. Soc. Rev.* **2014**, *43*, 8049–8080. [[CrossRef](#)] [[PubMed](#)]
11. Santos, R.M.; Audenaerde, A.V.; Chiang, Y.W.; Iacobescu, R.I.; Knops, P.; Gerven, T.V. Nickel extraction from olivine: Effect of carbonation pre-treatment. *Metals* **2015**, *5*, 1620–1644. [[CrossRef](#)]
12. Gislason, S.R.; Oelkers, E.H. Carbon storage in basalt. *Science* **2014**, *344*, 373. [[CrossRef](#)] [[PubMed](#)]
13. Matter, J.M.; Kelemen, P.B. Permanent storage of carbon dioxide in geological reservoirs by mineral carbonation. *Nat. Geosci.* **2009**, *2*, 837–841. [[CrossRef](#)]
14. Rigopoulos, I.; Delimitis, A.; Ioannou, I.; Efstathiou, A.M.; Kyratsi, T. Effect of ball milling on the carbon sequestration efficiency of serpentinized peridotites. *Miner. Eng.* **2018**, *120*, 66–74. [[CrossRef](#)]

15. Sanna, A.; Hall, M.R.; Maroto-Valer, M. Post-processing pathways in carbon capture and storage by mineral carbonation (CCSM) towards the introduction of carbon neutral materials. *Energy Environ. Sci.* **2012**, *5*, 7781–7796. [[CrossRef](#)]
16. Haug, A.H.; Kleiv, R.A.; Munz, I.A. Investigating dissolution of mechanically activated olivine for carbonation purposes. *Appl. Geochem.* **2010**, *25*, 1547–1563. [[CrossRef](#)]
17. Declercq, J.; Bosc, O.; Oelkers, E.H. Do organic ligands affect forsterite dissolution rates? *Appl. Geochem.* **2013**, *39*, 69–77. [[CrossRef](#)]
18. Li, J.; Hitch, M. Characterization of the microstructure of mechanically-activated olivine using X-ray diffraction pattern analysis. *Miner. Eng.* **2016**, *86*, 24–33. [[CrossRef](#)]
19. Rigopoulos, I.; Vasiliades, M.A.; Ioannou, I.; Efstathiou, A.M.; Godelitsas, A.; Kyratsi, T. Enhancing the rate of ex situ mineral carbonation in dunites. *Adv. Powder Technol.* **2016**, *27*, 360–371. [[CrossRef](#)]
20. Kleiv, R.A.; Thornhill, M. Mechanical activation of olivine. *Miner. Eng.* **2006**, *19*, 340–347. [[CrossRef](#)]
21. Kleiv, R.A.; Thornhill, M. The effect of mechanical activation in the production of olivine surface area. *Miner. Eng.* **2016**, *89*, 19–23. [[CrossRef](#)]
22. Baláž, P.; Turianicová, E.; Fabián, M.; Kleiv, R.A.; Briančin, J.; Obut, A. Structural changes in olivine (Mg,Fe)<sub>2</sub>SiO<sub>4</sub> mechanically activated in high-energy mills. *Int. J. Miner. Process.* **2008**, *88*, 1–6. [[CrossRef](#)]
23. Turianicová, E.; Baláž, P.; Tuček, L.; Zorkovská, A.; Zelenáček, V.; Németh, Z.; Šatka, A.; Kováč, J. A comparison of the reactivity of activated and non-activated olivine with CO<sub>2</sub>. *Int. J. Miner. Process.* **2013**, *123*, 73–77. [[CrossRef](#)]
24. Li, J.; Hitch, M. Mechanical activation of magnesium silicates for mineral carbonation: A review. *Miner. Eng.* **2018**, *128*, 69–83. [[CrossRef](#)]
25. Rigopoulos, I.; Petalidou, K.C.; Vasiliades, M.A.; Delimitis, A.; Ioannou, I.; Efstathiou, A.M.; Kyratsi, T. Carbon dioxide storage in olivine basalts: Effect of ball milling process. *Powder Technol.* **2015**, *273*, 220–229. [[CrossRef](#)]
26. Rigopoulos, I.; Harrison, A.L.; Delimitis, A.; Ioannou, I.; Efstathiou, A.M.; Kyratsi, T.; Oelkers, E.H. Carbon sequestration via enhanced weathering of peridotites and basalts in seawater. *Appl. Geochem.* **2018**, *91*, 197–207. [[CrossRef](#)]
27. Power, I.M.; Harrison, A.L.; Dipple, G.M.; Wilson, S.A.; Kelemen, P.B.; Hitch, M.; Southam, G. Carbon mineralization: from natural analogues to engineered systems. *Rev. Mineral. Geochem.* **2013**, *77*, 305–360. [[CrossRef](#)]
28. Wilson, S.A.; Harrison, A.L.; Dipple, G.M.; Power, I.M.; Barker, S.L.L.; Ulrich Mayer, K.; Fallon, S.J.; Raudsepp, M.; Southam, G. Offsetting of CO<sub>2</sub> emissions by air capture in mine tailings at the Mount Keith Nickel Mine, Western Australia: Rates, controls and prospects for carbon neutral mining. *Int. J. Greenh. Gas Control* **2014**, *25*, 121–140. [[CrossRef](#)]
29. Li, J.; Hitch, M. Ultra-fine grinding and mechanical activation of mine waste rock using a planetary mill for mineral carbonation. *Int. J. Miner. Process.* **2017**, *158*, 18–26. [[CrossRef](#)]
30. Li, J.; Hitch, M. Structural and chemical changes in mine waste mechanically-activated in various milling environments. *Powder Technol.* **2017**, *308*, 13–19. [[CrossRef](#)]
31. Li, J.; Hitch, M.; Power, I.M.; Pan, Y. Integrated mineral carbonation of ultramafic mine deposits—A review. *Minerals* **2018**, *8*, 147. [[CrossRef](#)]
32. Rigopoulos, I.; Vasiliades, M.A.; Petalidou, K.C.; Ioannou, I.; Efstathiou, A.M.; Kyratsi, T. A method to enhance the CO<sub>2</sub> storage capacity of pyroxenitic rocks. *Greenh. Gas. Sci. Technol.* **2015**, *5*, 1–14. [[CrossRef](#)]
33. Rigopoulos, I.; Petalidou, K.C.; Vasiliades, M.A.; Delimitis, A.; Ioannou, I.; Efstathiou, A.M.; Kyratsi, T. On the potential use of quarry waste material for CO<sub>2</sub> sequestration. *J. CO<sub>2</sub> Util.* **2016**, *16*, 361–370. [[CrossRef](#)]
34. Mukasa, S.B.; Ludden, J.N. Uranium–lead ages of plagiogranites from the Troodos ophiolite, Cyprus, and their tectonic significance. *Geology* **1987**, *1*, 825–828. [[CrossRef](#)]
35. Robinson, P.T.; Malpas, J. The Troodos Ophiolite of Cyprus: New perspectives on its origin and emplacement. In *Ophiolites: Oceanic Crustal Analogues*; Malpas, J., Moores, E.M., Panayiotou, A., Xenophontos, C., Eds.; Cyprus Geological Survey Department: Nicosia, Cyprus, 1990; pp. 13–36.
36. Robertson, A.H.F. Overview of the genesis and emplacement of Mesozoic ophiolites in the Eastern Mediterranean Tethyan region. *Lithos* **2002**, *65*, 1–67. [[CrossRef](#)]
37. Hochella, M.F.J. Nanogeoscience: From origins to cutting-edge applications. *Elements* **2008**, *4*, 373–379. [[CrossRef](#)]

38. Costa, C.N.; Anastasiadou, T.; Efstathiou, A.M. The selective catalytic reduction of nitric oxide with methane over La<sub>2</sub>O<sub>3</sub>–CaO systems: Synergistic effects and surface reactivity studies of NO, CH<sub>4</sub>, O<sub>2</sub>, and CO<sub>2</sub> by transient techniques. *J. Catal.* **2000**, *194*, 250–265. [CrossRef]
39. Efstathiou, A.M.; Bennett, C.O. Enthalpy and entropy of H<sub>2</sub> adsorption on Rh/Al<sub>2</sub>O<sub>3</sub> measured by Temperature-Programmed Desorption. *J. Catal.* **1990**, *124*, 116–126. [CrossRef]
40. Streckeisen, A.L. To each plutonic rock its proper name. *Earth Sci. Rev.* **1976**, *12*, 1–33. [CrossRef]
41. Munz, I.A.; Brandvoll, Ø.; Haug, T.A.; Iden, K.; Smeets, R.; Kihle, J.; Johansen, H. Mechanisms and rates of plagioclase carbonation reactions. *Geochim. Cosmochim. Acta* **2012**, *77*, 27–51. [CrossRef]
42. Rigopoulos, I.; Tsikouras, B.; Pomonis, P.; Hatzipanagiotou, K. Petrographic investigation of microcrack initiation in mafic ophiolitic rocks under uniaxial compression. *Rock Mech. Rock Eng.* **2013**, *46*, 1061–1072. [CrossRef]
43. Rigopoulos, I.; Tsikouras, B.; Pomonis, P.; Hatzipanagiotou, K. Microcracks in ultrabasic rocks under uniaxial compressive stress. *Eng. Geol.* **2011**, *117*, 104–113. [CrossRef]
44. Sissmann, O.; Brunet, F.; Martinez, I.; Guyot, F.; Verlaquet, A.; Pinquier, Y.; Daval, D. Enhanced olivine carbonation within a basalt as compared to single-phase experiments: reevaluating the potential of CO<sub>2</sub> mineral sequestration. *Environ. Sci. Technol.* **2014**, *48*, 5512–5519. [CrossRef] [PubMed]
45. Ounoughene, G.; Buskens, E.; Santos, R.M.; Cizer, Ö.; Gerven, T.V. Solvochemical carbonation of lime using ethanol: Mechanism and enhancement for direct atmospheric CO<sub>2</sub> capture. *J. CO<sub>2</sub> Util.* **2018**, *26*, 143–151. [CrossRef]
46. O'Connor, W.K.; Dahlin, D.C.; Rush, G.E.; Gerdemann, S.J.; Penner, L.R.; Nilsen, D.N. *Aqueous Mineral Carbonation: Mineral Availability, Pretreatment, Reaction Parameters, and Process Studies*; United States Department of Energy: Washington, DC, USA, 2005.
47. Rigopoulos, I.; Tsikouras, B.; Pomonis, P.; Hatzipanagiotou, K. The influence of alteration on the engineering properties of dolerites: The examples from the Pindos and Vourinos ophiolites (northern Greece). *Int. J. Rock Mech. Min. Sci.* **2010**, *47*, 69–80. [CrossRef]
48. Rigopoulos, I.; Tsikouras, B.; Pomonis, P.; Hatzipanagiotou, K. Assessment of the engineering behavior of ultramafic and mafic rocks using chemical alteration indices. *Eng. Geol.* **2015**, *196*, 222–237. [CrossRef]
49. Engidasew, T.A.; Barbieri, G. Geo-engineering evaluation of Termaber basalt rock mass for crushed stone aggregate and building stone from Central Ethiopia. *J. Afr. Earth Sci.* **2014**, *99*, 581–594. [CrossRef]
50. Rigopoulos, I.; Török, Á.; Kyratsi, T.; Delimitis, A.; Ioannou, I. Sustainable exploitation of mafic rock quarry waste for carbon sequestration following ball milling. *Resour. Policy* **2018**, in press. [CrossRef]
51. Intergovernmental Panel on Climate Change. *Guidelines for National Greenhouse Gas Inventories*; IPCC National Greenhouse Gas Inventories Programme: Hayama, Japan, 2006; Volume 3. Available online: [https://www.ipcc-nggip.iges.or.jp/public/2006gl/pdf/3\\_Volume3/V3\\_2\\_Ch2\\_Mineral\\_Industry.pdf](https://www.ipcc-nggip.iges.or.jp/public/2006gl/pdf/3_Volume3/V3_2_Ch2_Mineral_Industry.pdf) (accessed on 6 November 2018).
52. Hills, T.P.; Sceats, M.; Rennie, D.; Fennell, P. LEILAC: Low cost CO<sub>2</sub> capture for the cement and lime industries. *Energy Proc.* **2017**, *114*, 6166–6170. [CrossRef]

